


# Impact of population III stars on the astrophysical gravitational-wave background

Nikolaos Kouvatsos<sup>\*</sup> and Mairi Sakellariadou<sup>†</sup>

*Theoretical Particle Physics and Cosmology Group, Physics Department, King's College London,  
University of London, Strand, London WC2R 2LS, United Kingdom*

 (Received 9 April 2024; accepted 12 June 2024; published 12 July 2024)

We probe the astrophysical gravitational-wave background resulting from compact binary coalescences, focusing on population III binary black holes. We exploit results of state-of-the-art simulations on the evolution of population I-II and III binaries, considering a variety of initial condition and star formation rate models for the latter. The contribution from population III binary black holes is found to be very small, with no effect on the gravitational-wave spectrum. A network of third-generation detectors will detect easier individual population III binaries, due to their significantly higher masses, hence decreasing even further their residual contribution.

DOI: [10.1103/PhysRevD.110.023017](https://doi.org/10.1103/PhysRevD.110.023017)

## I. INTRODUCTION

During its first three observing runs, the LIGO-Virgo-KAGRA (LVK) collaboration has detected almost a hundred gravitational wave (GW) signals from compact binary coalescences (CBCs) [1–3], while at the end of the ongoing O4 run this number is expected to increase considerably [4]. This multitude of detections allows us to continuously refine our understanding of the stellar population of compact binaries and constrain astrophysical models. Apart from the transient signals, there is a continuous effort to search for the gravitational-wave background, a random signal made up of the superposition of numerous GWs throughout the history of the Universe [5,6].

While a gravitational-wave background may result from various cosmological mechanisms [7], the astrophysical GW background (AGWB) made up from CBC mergers is expected to be the dominant contributor [8,9]. To estimate the AGWB, only binaries produced by population I-II stars are usually considered. There is, however, an older population of stars—typically addressed in the literature as population III stars—which could result in a sizable contribution to the AGWB [10–13].

The increasing number of studies focusing on population III stars in recent years [14–28], combined with the updated information gained on population I and II

stars from the LVK collaboration detections, motivates us to revisit the AGWB from both population I-II and population III binaries. We compute the expected total AGWB from population I-II and III binaries for a network of 3G detectors, as well as the unresolved AGWB made up of binaries that are not individually detectable. We show that the contribution of GW signals from population III mergers to the total AGWB is negligible, as already found in previous studies [13]. We then show that since compact binaries from population III stars are expected to be much more massive than those of population I-II stars, hence easier to be detected individually in the astrophysical GW *foreground*, their contribution to the AGWB is completely lost after foreground subtraction.

This paper is organized as follows. In Sec. II, we revisit the standard formalism to study the AGWB, focusing on an approach with catalogs of sources. We then describe the simulated population models and the corresponding compact binary parameters. In Sec. III, we outline the process to remove the astrophysical GW foreground detected by a 3G detector network. In Sec. IV we present our findings for the total and unresolved AGWB. We also discuss statistics for population I-II and III binaries in terms of the signal-to-noise ratio. In Sec. V, we summarize our conclusions and briefly comment on the differences between our and related previous studies.

## II. ASTROPHYSICAL GRAVITATIONAL-WAVE BACKGROUND

We briefly outline the formalism to estimate the AGWB. We then summarize our method to build catalogs of compact binaries and highlight our selected binary parameters.

<sup>\*</sup>Contact author: [nikolaos.kouvatsos@kcl.ac.uk](mailto:nikolaos.kouvatsos@kcl.ac.uk)

<sup>†</sup>Contact author: [mairi.sakellariadou@kcl.ac.uk](mailto:mairi.sakellariadou@kcl.ac.uk)

*Published by the American Physical Society under the terms of the Creative Commons Attribution 4.0 International license. Further distribution of this work must maintain attribution to the author(s) and the published article's title, journal citation, and DOI.*

### A. Formalism

We describe the AGWB by the normalized GW energy spectrum [29],

$$\Omega_{\text{GW}}(f) = \frac{1}{c^2 \rho_c} \frac{d\rho_{\text{GW}}}{d \ln f} = \frac{f}{c^3 \rho_c} F(f), \quad (1)$$

where  $\rho_c = 3H_0^2/(8\pi G)$  is the critical energy density, with  $H_0$  the Hubble's constant and  $G$  the Newton's gravitational constant,  $c$  the speed of light, and  $f$  the GW frequency in the detector frame. The integrated flux density [30],

$$F(f) = \int_0^{z_{\text{max}}} \frac{R(z)}{4\pi d_c^2(z)} \frac{dE_{\text{GW}}}{df_s} \Big|_{f_s} dz, \quad (2)$$

depends on the merger rate,  $R(z)$ , the comoving distance,  $d_c(z)$ , and the GW energy spectrum in the source frame,  $dE_{\text{GW}}/df_s$ , with  $f_s = f(1+z)$  the GW frequency in the source frame. We express the merger rate  $R(z)$  in terms of the merger rate per unit comoving volume,  $R_V(z)$ , as

$$R(z) = \frac{R_V(z) dV}{1+z dz} = \frac{4\pi c}{H_0} \frac{R_V(z) d_c^2(z)}{(1+z)E(z)}, \quad (3)$$

where  $E(z) = \sqrt{\Omega_m(1+z)^3 + \Omega_\Lambda}$ . We adopt a flat  $\Lambda$ CDM model with  $\Omega_m = 0.31$ ,  $\Omega_\Lambda = 0.69$ , and  $H_0 = 67.66$  km/s/Mpc [31]. The  $(1+z)$  factor accounts for cosmic expansion.

The GW energy spectrum for a single source reads [32]

$$\frac{dE_{\text{GW}}}{df_s} \Big|_{f_s} = \frac{2\pi^2 d_c^2 c^3}{G} f_s^2 \left( |\tilde{h}_+(f_s)|^2 + |\tilde{h}_\times(f_s)|^2 \right), \quad (4)$$

where  $\tilde{h}_+$ ,  $\tilde{h}_\times$  are the Fourier transforms of the two polarization modes of the gravitational waveform in the frequency domain.

Given a catalog of sources, the GW energy spectrum, Eq. (4), can be computed for each source individually. The integrated flux density, Eq. (2), can then be replaced by a sum over all sources [33]:

$$F(f) = \frac{1}{T} \frac{\pi c^3}{2G} f^2 \sum_{i=1}^N \left( |\tilde{h}_+^i(f)|^2 + |\tilde{h}_\times^i(f)|^2 \right), \quad (5)$$

where  $\tilde{h}_+$ ,  $\tilde{h}_\times$  are now taken in the detector frame, where  $i$  denotes a particular source. The total number of sources,  $N$ , is related to the total time of observation,  $T$ , as

$$N = T \int_0^{z_{\text{max}}} \frac{R_V(z) dV}{1+z dz} = T \int_0^{z_{\text{max}}} \frac{4\pi c}{H_0} \frac{R_V(z) d_c^2(z)}{(1+z)E(z)} dz. \quad (6)$$

In what follows, we use catalogs of simulated GW sources, which have been stored in redshift bins. We thus

perform a discrete summation to calculate  $N$ , instead of computing the integral expression given in Eq. (6). The number of sources at each redshift bin is then given by

$$N_i = T \frac{4\pi c}{H_0} \frac{R_V(z_i) d_c^2(z_i)}{(1+z_i)E(z_i)} \Delta z_i, \quad (7)$$

with total number of sources

$$N = \sum_i^{z_{\text{max}}} N_i. \quad (8)$$

We opt for a redshift resolution  $\Delta z_i = 0.1$ ,  $\forall i$  and fix  $N = 10^5$  for statistical convergence (as in Ref. [34]).

### B. Catalogs

We use binaries simulated and evolved utilizing the *Stellar Evolution for N-body* (SEVN) binary population synthesis code [35–37]. We make a distinction between population I-II and population III binaries. For the former, we pick the *Fiducial* model from Ref. [37], for three distinct classes of compact binaries: binary black holes (BBHs), black hole–neutron stars (BHNSs), and binary neutron stars (BNSs). For the latter, we use results from Ref. [27] (in which only BBHs have been produced<sup>1</sup>), considering 11 distinct models, each assuming different initial conditions (ICs) (denoted by *LOG1*, *LOG2*, *LOG3*, *LOG4*, *LOG5*, *KRO1*, *KRO5*, *LAR1*, *LAR5*, *TOP1*, *TOP5*).

The SEVN binary population synthesis code, provides three of the binary parameters, namely, the two compact binary masses and the eccentricity of the orbit.

The star formation rate (SFR) is expected to be different for population I-II and population III stars, based on their different metallicity. For the former, we consider the metallicity-dependent Madau-Fragos SFR model [38], with metallicity bins:  $Z \in \{0.0001, 0.0002, 0.0004, 0.0006, 0.0008, 0.001, 0.002, 0.004, 0.006, 0.008, 0.01, 0.014, 0.017, 0.02, 0.03\}$  [26]. For the latter, we consider four different SFR models [39–42] (denoted by *H22*, *J19*, *LB20*, *SW20* in Ref. [26]), all with the same metallicity  $Z = 10^{-11}$  [26].

The high number of considered IC and SFR models aims to account for the high uncertainty that characterizes the properties of population III stars. For a brief description of the different models, see Appendix A.

Once we have the star formation rate (SFR), we use the (publicly available) code COSMORATE [43,44] to get—for a given redshift bin—the merger rate density (MRD) and a set of binaries, from which we randomly select  $N_i$ , Eq. (7), to produce a catalog.

<sup>1</sup>Past studies on supernova remnants from population III have focused on black holes, which is why we choose to neglect the contributions to the  $\Omega_{\text{GW}}$  from the BHNS and BNS subpopulations as subdominant. We refer the reader to Refs. [14–28].

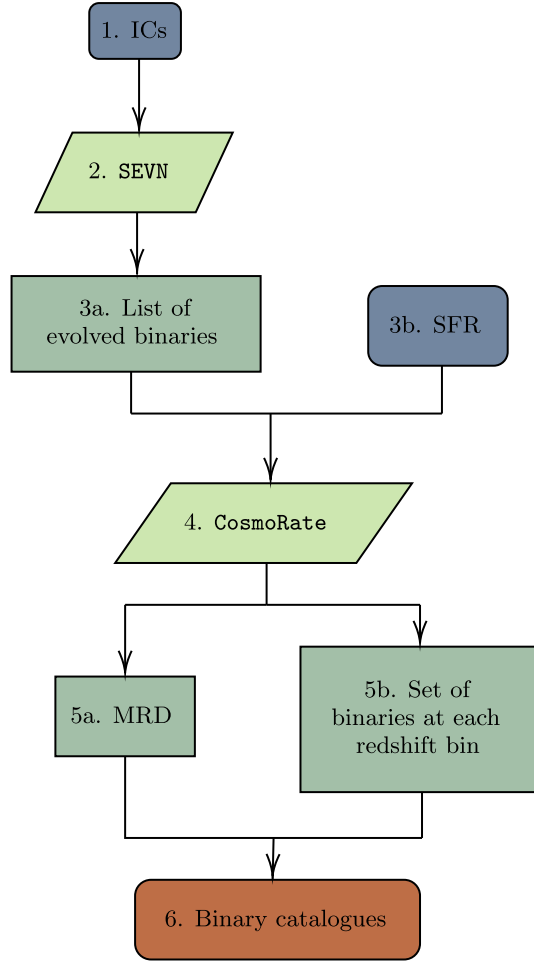


FIG. 1. Flowchart summarising the steps followed to construct the binary catalogues, for a model with given initial conditions (ICs) and star formation rate (SFR). Steps 1-3a have already been performed in Ref. [27,37]. The list of evolved binaries (step 3a) can be found in Ref. [45,46].

The aforementioned steps to produce a catalog are summarized in the flowchart, Fig. 1.

As mentioned previously, SEVN provides only the compact binary masses in the source frame,  $m_{1(\text{source})}$  and  $m_{2(\text{source})}$  (where 1 stands for the primary and 2 for the secondary compact object), and the eccentricity,  $e$ . We have to choose eight additional parameters: two intrinsic parameters (spins) and six extrinsic ones (polarization angle, coalescence phase, right ascension, declination, inclination angle, and coalescence time). We sample as follows (see Table I):

- (i) The spins in the  $z$  direction,  $\chi_{1(z)}$  and  $\chi_{2(z)}$ , are sampled from uniform distributions in the range  $[-0.75, 0.75]$  for black holes, and  $[-0.05, 0.05]$  for neutron stars [47]. We set the spins in the  $x$  and  $y$  direction to 0.
- (ii) The polarization angle,  $\psi$ , coalescence phase,  $\phi_c$ , right ascension,  $\alpha$ , declination,  $\delta$ , and inclination

TABLE I. Summary of the distributions we use to sample in all compact binary parameters.

Parameter	Sampling distributions	
	Black holes	Neutron stars
$m_{1(\text{source})}, m_{2(\text{source})}, e, z$	SEVN and COSMORATE	
$\chi_{1(x)}, \chi_{1(y)}, \chi_{2(x)}, \chi_{2(y)}, t_c$	0	
$\chi_{1(z)}, \chi_{2(z)}$	Uniform in $[-0.75, 0.75]$	Uniform in $[-0.05, 0.05]$
$\psi, \alpha, \phi_c$	Uniform in $[0, 2\pi]$	
$\cos(\iota), \cos(\delta + \pi/2)$	Uniform in $[-1, 1]$	

angle,  $\iota$  are sampled from uniform distributions in  $\psi$ ,  $\alpha$ ,  $\phi_c$ ,  $\cos(\iota)$ ,  $\cos(\delta + \pi/2)$ .

- (iii) The coalescence time in the detector data segment,  $t_c$ , is set at 0 for all signals.

As for the gravitational waveform we use to model the signals, we have opted for IMRPHENOMXHM [48]. This choice has been motivated by a preference for probing the harmonic modes of the signals to compute the AGWB (as considered in Ref. [12]), rather than precession.

### III. UNRESOLVED AGWB

An AGWB present in the data will be dominated by a foreground of loud detected signals; removing them from the dataset would allow to estimate the AGWB truly composed of individually unresolvable signals.

The unresolved contribution to the  $\Omega_{\text{GW}}$  is made up of all signals below some SNR threshold. For the  $i$ th binary, we define the network optimal SNR as

$$\rho_i^2 = \sum_{I=1}^M 4 \int_{f_{\min}}^{f_{\max}} \frac{|\tilde{H}_I^i(f)|^2}{P_I(f)} df, \quad (9)$$

where

$$\begin{aligned} \tilde{H}_I^i(f) = & F_{\text{lp}}^{l,i}(f, \alpha_i, \delta_i) [F_+^{l,i}(f, \alpha_i, \delta_i, \psi_i) \tilde{h}_+^i(f) \\ & + F_\times^{l,i}(f, \alpha_i, \delta_i, \psi_i) \tilde{h}_\times^i(f)] \end{aligned} \quad (10)$$

is the detector response,  $P_I$  the power spectral density (PSD) of detector  $I$ , and  $M$  the total number of considered detectors. We denote by  $F_{\text{lp}}$  the location-phase factor, and by  $F_+$ ,  $F_\times$  the antenna pattern functions.

We consider a three 3G detector network: an L-shaped Cosmic Explorer (CE) detector with 20 km-long arms and postmerger optimized PSD located at the site of LIGO Hanford, an L-shaped CE detector with 40 km-long arms and compact-binary optimized PSD located at the site of LIGO Livingston [49], and a triangular (that is, composed of three distinct interferometers) Einstein Telescope (ET) detector with 10 km-long arms located at the site of

Virgo [50]. We set the minimum frequency at  $f_{\min} = 5$  Hz and the maximum frequency at  $f_{\max} = 1024$  Hz [51], as contributions to the SNR outside this frequency range are negligible. To compute the SNR we use the `GWBENCH` package [52].

We compute the optimal SNR of every signal in our catalog. The calculation of the unresolved AGWB follows the same procedure as outlined for the total AGWB, with the sole difference that this time we only consider the signals in our catalogs that pass the SNR threshold. We consider two choices for the SNR threshold:  $\rho_{\text{thr}} = 12$  (conservative), and  $\rho_{\text{thr}} = 8$ .

## IV. RESULTS

In what follows, we present the total AGWB produced separately by mergers of population I-II stars and population III stars, and discuss the characteristics of the latter versus the former. We then discuss the difference in the unresolved AGWB for population I-II versus population III, noting that this depends on the detector sensitivities. In our study, we have used a three 3G detector network and fixed the SNR threshold.

### A. Total background

We plot in Fig. 2 the total  $\Omega_{\text{GW}}$  from mergers of all three binary classes (BBHs, BHNSs, and BNSs) produced by population I-II stars, as well as the individual contributions. We also plot the  $\Omega_{\text{GW}}$  resulting from population III binaries, considering the most optimistic (*J19*, *LARI*) and most pessimistic (*SW20*, *TOP5*) cases (we refer the reader to Appendix B, where we present results for all population III cases). We also show the total AGWB from population I-II, and III binaries, where for the latter we selected the most optimistic model.

We observe that for population I-II, the BHNS contribution is the weakest. The AGWB seems to be dominated by the BBH mergers in the whole frequency range except for the highest frequencies, above  $f \sim 900$  Hz, where the BNS contribution prevails. The contribution from population III binaries peaks at  $\sim 10^{-13}$  or  $\sim 6 \times 10^{-11}$  depending on the assumed SFR and IC model. In all cases, we observe a plateau which in the most optimistic scenario is in the region  $f \in [20, 200]$  Hz. Clearly, even in this most optimistic case, the resulting increase in the total AGWB after including BBHs from population III stars is only minimal, hence insufficient to lead to significant deviation from the expected  $\propto f^{2/3}$  spectrum [32]. Considering the contribution from population I-II and III binaries, the  $\Omega_{\text{GW}}$  peaks just above  $10^{-9}$ .

We next investigate the AGWB from population I-II and population III binaries when considering only unresolved sources.

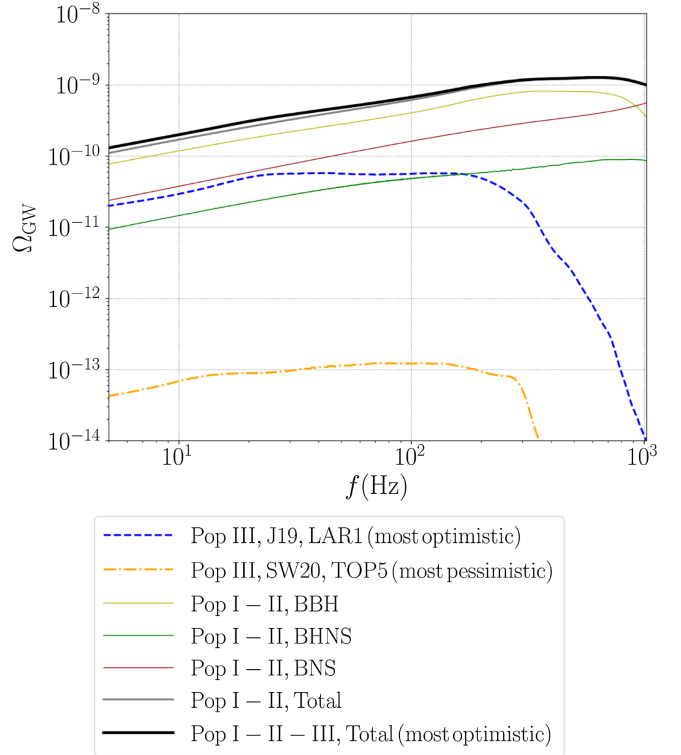


FIG. 2. The AGWB resulting from mergers of BBHs, BHNSs, and BNSs produced by population I-II stars, as well as their total. Including the BBH mergers from population III stars has a negligible impact even when considering the most optimistic model. The AGWB for the most pessimistic population III model is also provided for comparison.

### B. Unresolved background

We plot in Fig. 3 the unresolved AGWB for our two choices of  $\rho_{\text{thr}}$ . First, we consider the population I-II contribution. Imposing an SNR threshold of 12 seems to drop the  $\Omega_{\text{GW}}$  by  $\sim 1$  order of magnitude in the whole frequency range except for the highest frequencies, where the BNS mergers contribute most. This is expected, as GW signals from BNSs are weaker than those from BBHs and dominate after foreground subtraction.

We next consider population III for the most optimistic case (*J19*, *LARI*). One would expect BBH mergers from population III stars to be overall harder to detect than those of population I-II stars, given that the merger rate density for population III binaries peaks at higher redshifts (see Appendix B for a detailed figure of the computed MRD). We observe, however, that the corresponding unresolved  $\Omega_{\text{GW}}$ , for an SNR threshold of 12, lies  $\sim 2$  orders of magnitude below the total  $\Omega_{\text{GW}}$  for  $f \leq 30$  Hz, where it follows the  $\propto f^{2/3}$  dependence. Notice that  $\Omega_{\text{GW}}$  has lost its characteristic plateau, dropping abruptly for frequencies above  $f \sim 30$  Hz. Such frequencies correspond to BBHs

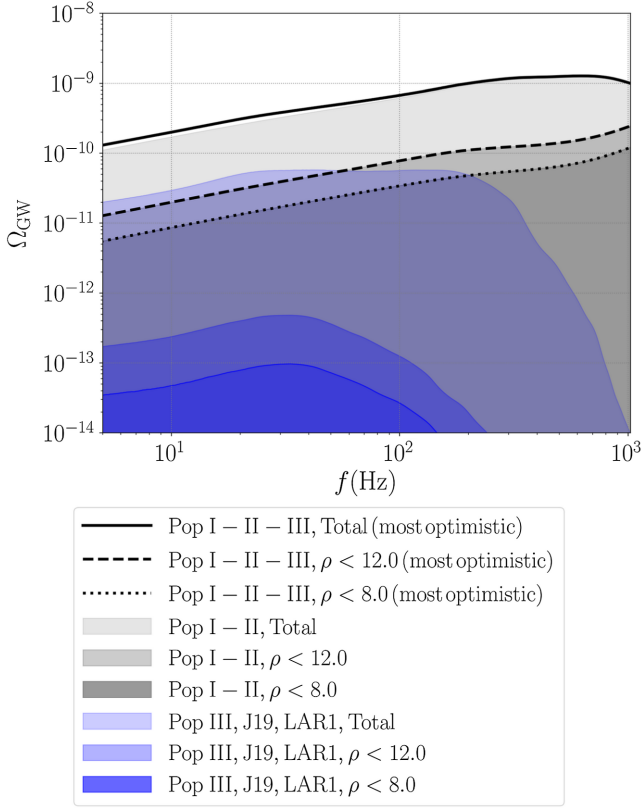


FIG. 3. The unresolved AGWB resulting from mergers of binaries produced by population I-II and III stars, for an SNR threshold  $\rho_{\text{thr}} \in \{8, 12\}$ . The AGWB before the foreground subtraction is also plotted for comparison. Removing the foreground of unresolvable sources from our catalog seems to reduce the AGWB more in the case of population III binaries. Finally, we provide the total AGWB from all three populations before and after the foreground subtraction.

with very low redshifts, thus high SNRs, therefore removed by the foreground subtraction.

To further quantify the difference in the foreground subtraction between population I-II and III binaries, we show in Fig. 4 a histogram of the network optimal SNRs for BBH mergers from population I-II and III (*J19*, *LAR1*) binaries. The SNR distribution for population III appears noticeably shifted towards higher SNRs compared to the same distribution for population I-II, with a mean SNR of 38.0 instead of 27.3, respectively. It is, therefore, sensible that in the case of population III the deviation of the unresolved AGWB from the total one is greater.

Note that these results assume a perfect foreground subtraction. Even though this is not the case [34,53], we are not considering any errors that would decrease the efficiency of the subtraction, since the contribution from population III binaries to the total AGWB is quite small, and lost after foreground subtraction.

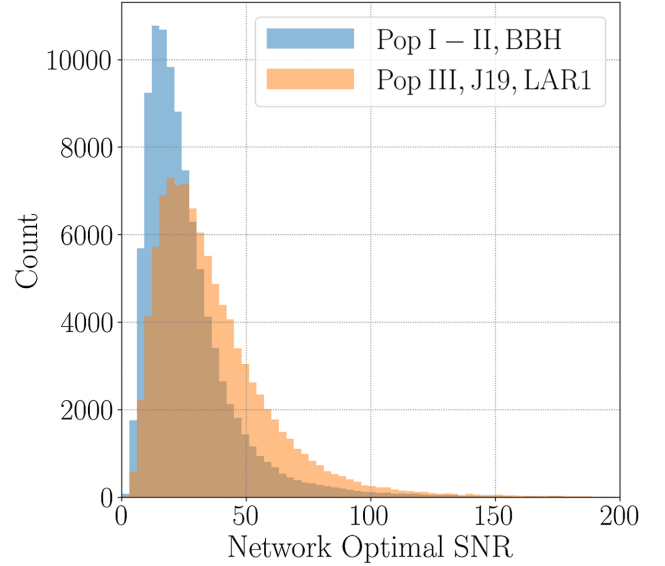


FIG. 4. Histogram with the network optimal SNRs of all BBHs for population I-II and population III (*J19*, *LAR1*). Despite the higher redshifts typically associated with population III BBHs compared to population I-II, the distribution of the former is shifted towards higher SNRs due their significantly higher masses.

## V. DISCUSSION AND CONCLUSIONS

We have studied the contribution from population III compact binaries mergers to the astrophysical gravitational-wave background and compared to that from population I-II. For population I-II binaries, we have considered all three types of mergers (BBH, BNS, BHNS). For population III, we have considered a variety of models with different initial conditions for the binary population synthesis code and different star formation rate.

Our analysis has determined that including GW signals from population III binaries has a very small impact on the total  $\Omega_{\text{GW}}$ , as already shown in Ref. [12]. Our study, however, has yielded results that contradict expectations on the unresolved AGWB. Specifically, we find population III binaries to be on average easier to detect than population I-II binaries, regardless of the assumed initial conditions and star formation rate of the former. For a given SNR threshold, foreground subtraction has a greater impact in the case of population III binaries, resulting in their contribution to the total AGWB being lost. Hence, the AGWB is characterized and distinguished from the cosmological GWB by its  $\propto f^{2/3}$  spectrum. Loud individual GW signals from population III binaries could be present in the data and identifiable from their higher redshifts compared to population I-II binaries.

Let us note that the difference in our results with respect to previous ones [12,13] is due mainly to the different merger rates and binary masses of the considered catalogs. To build our catalogs, we have employed results from the

SEVN binary population synthesis code, whereas the study of Refs. [12,13] is based on simulations with STARTRACK [54]. We refer the reader to models *M10* and *FSI* for population I-II and III, respectively, of Ref. [18]. In our models the MRD peaks at  $z \simeq 4.5$  and  $z \geq 7.5$  for population I-II and population III, respectively, whereas for the STARTRACK models the MRD peaks correspondingly at  $z \simeq 2$  and  $z \simeq 12$ . For our models, the average BBH total source mass is  $M_{\text{source}} = 16.8M_{\odot}$  for population I-II, and ranges from  $M_{\text{source}} = 49.6M_{\odot}$  (*H22*, *KRO1*) to  $M_{\text{source}} = 64.0M_{\odot}$  for population III binaries (see Appendix B for a detailed figure of the total source mass distribution), whereas for the STARTRACK models the corresponding masses (for mergers within  $z < 2$ ) are  $M_{\text{source}} = 29.7M_{\odot}$  and  $M_{\text{source}} = 63.4M_{\odot}$ . Finally, we note that the BHNS and BNS waveform adopted in Refs. [12,13] considered only the inspiral phase.

## ACKNOWLEDGMENTS

We had a number of fruitful discussions on the subject of this paper with Chris Belczynski, now deceased. This material is based upon work supported by NSF’s LIGO Laboratory, which is a major facility fully funded by the National Science Foundation. The authors acknowledge computational resources provided by the LIGO Laboratory and supported by NSF Grants No. PHY-0757058 and No. PHY-0823459. We are indebted to Filippo Santoliquido for many useful discussions on population III stars. We also thank Ssohrab Borhanian for suggestions on how to run GWBENCH. N. K. thanks Ansh Gupta, Claire Rigouzzo, and Michelle Gurevich, and M. S. thanks Tania Regimbau for discussions. We thank Nelson Christensen for carefully reviewing this work as a part of the LVK collaboration’s internal review process. N. K. is supported by King’s College London through an NMES Funded Studentship. M. S. acknowledges support from the Science and Technology Facility Council (STFC), UK, under the Research Grant No. ST/X000753/1. This manuscript was assigned LIGO-Document No. P2400127.

## APPENDIX A: DIFFERENCES IN POPULATION III MODELS

### 1. Initial conditions

#### a. Initial mass function

The initial mass function (IMF) for population III stars is expected to be quite top heavy, compared to the one for population I-II stars [55–61]. This is because the former are characterized by extremely low metallicity and molecular hydrogen is an inefficient coolant, compared to heavier elements [57,62–72]. All considered IMFs favor lower masses, and are essentially power laws [40,63,63–71,73–75] (for some models [40,63,74,75] multiplied by an exponential at the lower edge). The most optimistic scenario is given by an IMF which is almost constant [40,63,75]. The

aforementioned IMFs were used to sample in primary mass in Ref. [27].

### b. Mass ratio and secondary mass

The secondary mass distribution was either identical to the primary mass distribution, or determined assuming a power law distribution [63,76] for the mass ratio. In both cases, the final mass ratio distribution also depends on the primary mass distribution.

### c. Orbital period

The orbital period distribution is either a power law favoring shorter periods [76], or a Gaussian distribution [63].

### d. Eccentricity

The eccentricity distribution is a power law with either positive [15,16,20] or negative [76] exponent, favoring either higher or lower eccentricities, respectively.

## 2. Star formation rate

All considered models for the star formation rate are consistent with the Thomson scattering optical depth value estimated by the Planck collaboration [77]. Their peak varies significantly, from  $z \simeq 8$  (*J19*) to  $z \simeq 20$  (*SW20*), depending on different physical assumptions. First, *H22* is a semianalytic model that samples and traces individual stars, based on dark matter halo merger trees and calibrated to reproduce observables in the Universe [78,79]. Next, *J19* was obtained using the hydrodynamical/ $N$ -body code GIZMO [80], considering both the chemical and radiative feedback of core-collapse and pair-instability supernovae. Likewise, *LB20* was the result of simulations with GIZMO, extrapolated to lower redshifts and following a Madau-Dickinson form [81]. Finally, *SW20* was constructed from hydrodynamical cosmological simulations that ran on the adaptive mesh refinement code ENZO [82].

## APPENDIX B: ADDITIONAL RESULTS

### 1. Total background

We plot in Fig. 5 the  $\Omega_{\text{GW}}$  from population III BBH mergers, for the four SFR models discussed in Sec. II B. Each of the four panels considers a single SFR model (listed at the top left corner), and 11 different IC models. Note that the individual curves appear, in general, wobbly in the region  $f \geq 200$  Hz. This is because high frequencies in the  $\Omega_{\text{GW}}$  correspond to signals that are emitted by low redshift sources, which are inevitably few in our catalogs. Thus,  $\Omega_{\text{GW}}$  at these frequencies is characterized by higher statistical uncertainties. Notice that in all cases there is a plateau, as discussed in Sec. IV A.

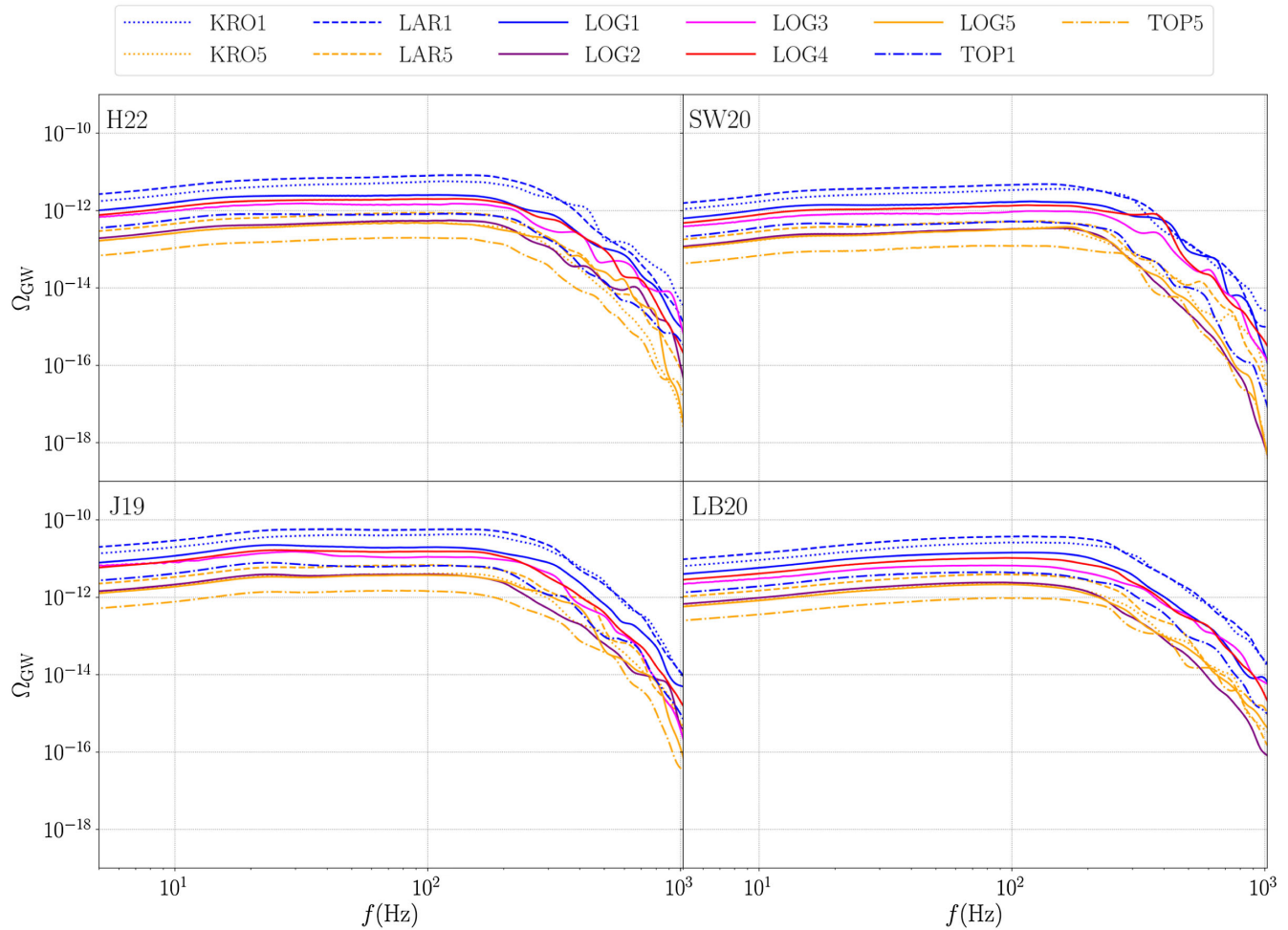


FIG. 5. The GWB resulting from mergers of BBHs produced by population III stars, for four different SFR models (four subfigures) and 11 different initial condition models. All models have been taken from [26,27].

## 2. Merger rate density

We show in Fig. 6 the MRD over redshift for population I-II and population III BBHs. Even in the most optimistic case (*J19*, *LAR1*), the population III MRD peak value ( $70.6 \text{ Gpc}^{-3} \text{ yr}^{-1}$ ) is significantly lower than the one for population I-II BBH MRD peak value ( $172.2 \text{ Gpc}^{-3} \text{ yr}^{-1}$ ), and lies at a much higher redshift (4.55 and 7.65, respectively). In all other cases, the MRD peaks at  $z \geq 7.65$ .

## 3. Mass distribution

We plot in Fig. 7 the total source mass distribution for population I-II and population III BBHs. This is expected

to be generally higher for the latter because of the corresponding extremely low metallicity, which implies that (a) the initial mass function is more top heavy as compared to metal-rich stars and (b) there is virtually no mass lost in stellar winds [83,84]. Indeed, the  $M_{\text{source}}$  distribution takes typically higher values for all population III models compared to population I-II. Interestingly, we notice that (*J19*, *LAR1*), which appears rather pessimistic in terms of the expected  $M_{\text{source}}$ , turns out to be the most optimistic case in terms of the  $\Omega_{\text{GW}}$  (as seen in Fig. 5) as a result of its high MRD. Note that the fast drop around  $M_{\text{source}} \sim 100$  can be associated to the pair-instability mass gap, which for population III BBHs simulated with SEVN has a lower edge at  $M_{\text{source}} = 86M_{\odot}$  [27].

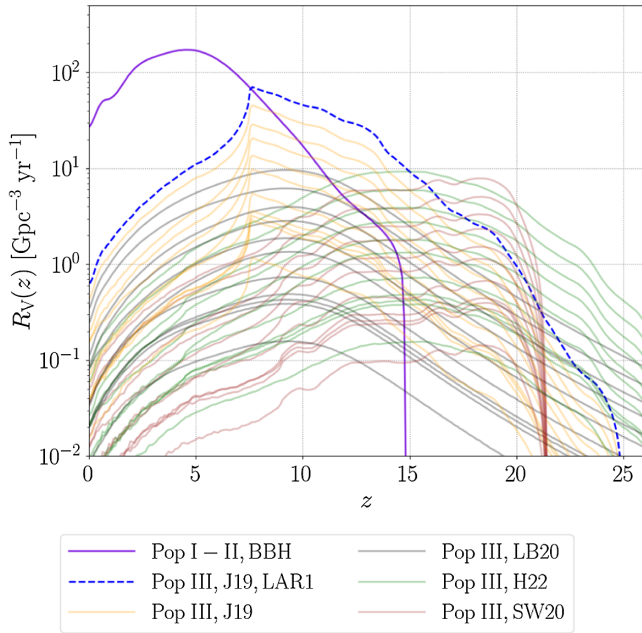


FIG. 6. The BBH merger rate density (MRD) for population I-II and the *J19*, *LAR1* population III model, as computed using COSMORATE. The MRD for every other population III model is also plotted.

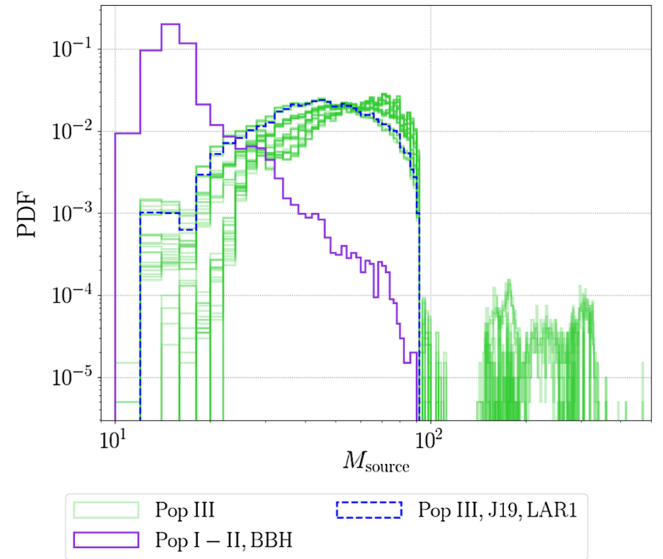


FIG. 7. The BBH total source mass distribution for population I-II and the *J19*, *LAR1* population III model. The latter is clearly characterized by more massive, on average, BBHs. The  $M_{\text{source}}$  distribution for every other population III model is also plotted.

- [1] LIGO Scientific and Virgo Collaborations, GWTC-1: A gravitational-wave transient catalog of compact binary mergers observed by LIGO and Virgo during the first and second observing runs, *Phys. Rev. X* **9**, 031040 (2019).
- [2] LIGO Scientific and Virgo Collaborations, GWTC-2: Compact binary coalescences observed by LIGO and Virgo during the first half of the third observing run, *Phys. Rev. X* **11**, 021053 (2021).
- [3] LIGO Scientific, Virgo, and KAGRA Collaborations, GWTC-3: Compact binary coalescences observed by LIGO and Virgo during the second part of the third observing run, *Phys. Rev. X* **13**, 041039 (2023).
- [4] LIGO Scientific, Virgo, and KAGRA Collaborations, Prospects for observing and localizing gravitational-wave transients with Advanced LIGO, Advanced Virgo and KAGRA, *Living Rev. Relativity* **21**, 3 (2018).
- [5] B. Allen, The stochastic gravity-wave background: Sources and detection, in *Proceedings of Les Houches School of Physics: Astrophysical Sources of Gravitational Radiation*, edited by J.-A. Marck and J.-P. Lasota (Cambridge Contemporary Astrophysics, 1997), pp. 373–417; J.-A. Marck and J.-P. Lasota, [arXiv:gr-qc/9604033](https://arxiv.org/abs/gr-qc/9604033).
- [6] N. Christensen, Stochastic gravitational wave backgrounds, *Rep. Prog. Phys.* **82**, 016903 (2018).
- [7] C. Caprini and D. G. Figueroa, Cosmological backgrounds of gravitational waves, *Classical Quantum Gravity* **35**, 163001 (2018).
- [8] T. Regimbau and V. Mandic, Astrophysical sources of stochastic gravitational-wave background, *Classical Quantum Gravity* **25**, 184018 (2008).
- [9] T. Regimbau, The astrophysical gravitational wave stochastic background, *Res. Astron. Astrophys.* **11**, 369 (2011).
- [10] I. Kowalska, T. Bulik, and K. Belczynski, Gravitational wave background from population III binaries, *Astron. Astrophys.* **541**, A120 (2012).
- [11] K. Inayoshi, K. Kashiyama, E. Visbal, and Z. Haiman, Gravitational wave background from population III binary black holes consistent with cosmic reionization, *Mon. Not. R. Astron. Soc.* **461**, 2722 (2016).
- [12] C. Périgois, C. Belczynski, T. Bulik, and T. Regimbau, STARTRACK predictions of the stochastic gravitational-wave background from compact binary mergers, *Phys. Rev. D* **103**, 043002 (2021).
- [13] K. Martinovic, C. Périgois, T. Regimbau, and M. Sakellariadou, Footprints of population III stars in the gravitational-wave background, *Astrophys. J.* **940**, 29 (2022).
- [14] K. Belczynski, T. Bulik, and B. Rudak, The first stellar binary black holes: The strongest gravitational wave burst sources, *Astrophys. J.* **608**, L45 (2004).



- [15] T. Kinugawa, K. Inayoshi, K. Hotokezaka, D. Nakauchi, and T. Nakamura, Possible indirect confirmation of the existence of Pop III massive stars by gravitational wave, *Mon. Not. R. Astron. Soc.* **442**, 2963 (2014).
- [16] T. Hartwig, M. Volonteri, V. Bromm, R. S. Klessen, E. Barausse, M. Magg, and A. Stacy, Gravitational waves from the remnants of the first stars, *Mon. Not. R. Astron. Soc.* **460**, L74 (2016).
- [17] K. Inayoshi, R. Hirai, T. Kinugawa, and K. Hotokezaka, Formation pathway of population III coalescing binary black holes through stable mass transfer, *Mon. Not. R. Astron. Soc.* **468**, 5020 (2017).
- [18] K. Belczynski, T. Ryu, R. Perna, E. Berti, T. L. Tanaka, and T. Bulik, On the likelihood of detecting gravitational waves from Population III compact object binaries, *Mon. Not. R. Astron. Soc.* **471**, 4702 (2017).
- [19] T. Kinugawa, T. Nakamura, and H. Nakano, Chirp mass and spin of binary black holes from first star remnants, *Mon. Not. R. Astron. Soc.* **498**, 3946 (2020).
- [20] A. Tanikawa, H. Susa, T. Yoshida, A. A. Trani, and T. Kinugawa, Merger rate density of population III binary black holes below, above, and in the pair-instability mass gap, *Astrophys. J.* **910**, 30 (2021).
- [21] A. Tanikawa, T. Kinugawa, T. Yoshida, K. Hijikawa, and H. Umeda, Population III binary black holes: Effects of convective overshooting on formation of GW190521, *Mon. Not. R. Astron. Soc.* **505**, 2170 (2021).
- [22] T. Kinugawa, T. Nakamura, and H. Nakano, Formation of binary black holes similar to GW190521 with a total mass of  $\sim 150M_{\odot}$  from population III binary star evolution, *Mon. Not. R. Astron. Soc.* **501**, L49 (2020).
- [23] T. Kinugawa, T. Nakamura, and H. Nakano, Formation of mass gap compact object and black hole binary from population III stars, *Prog. Theor. Exp. Phys.* **2021**, 021E01 (2020).
- [24] T. Kinugawa, T. Nakamura, and H. Nakano, Gravitational waves from population III binary black holes are consistent with LIGO/Virgo O3a data for the chirp mass larger than  $\sim 20M_{\odot}$ , *Mon. Not. R. Astron. Soc.* **504**, L28 (2021).
- [25] A. Tanikawa, G. Chiaki, T. Kinugawa, Y. Suwa, and N. Tominaga, Can population III stars be major origins of both merging binary black holes and extremely metal poor stars?, *Publ. Astron. Soc. Jpn.* **74**, 521 (2022).
- [26] F. Santoliquido, M. Mapelli, G. Iorio, G. Costa, S. C. O. Glover, T. Hartwig, R. S. Klessen, and L. Merli, Binary black hole mergers from population III stars: Uncertainties from star formation and binary star properties, *Mon. Not. R. Astron. Soc.* **524**, 307 (2023).
- [27] G. Costa, M. Mapelli, G. Iorio, F. Santoliquido, G. J. Escobar, R. S. Klessen, and A. Bressan, Massive binary black holes from population II and III stars, *Mon. Not. R. Astron. Soc.* **525**, 2891 (2023).
- [28] A. Tanikawa, Contribution of population III stars to merging binary black holes, *Rev. Mod. Plasma Phys.* **8**, 13 (2024).
- [29] B. Allen and J. D. Romano, Detecting a stochastic background of gravitational radiation: Signal processing strategies and sensitivities, *Phys. Rev. D* **59**, 102001 (1999).
- [30] T. Regimbau and V. Mandic, Astrophysical sources of stochastic gravitational-wave background, *Classical Quantum Gravity* **25**, 184018 (2008).
- [31] Planck Collaboration, Planck 2018 results. VI. Cosmological parameters, *Astron. Astrophys.* **641**, A6 (2020).
- [32] E. S. Phinney, A practical theorem on gravitational wave backgrounds, <https://api.semanticscholar.org/CorpusID:18174165> (2001).
- [33] T. Regimbau, M. Evans, N. Christensen, E. Katsavounidis, B. Sathyaprakash, and S. Vitale, Digging deeper: Observing primordial gravitational waves below the binary-black-hole-produced stochastic background, *Phys. Rev. Lett.* **118**, 151105 (2017).
- [34] B. Zhou, L. Reali, E. Berti, M. Çalıřkan, C. Creque-Sarbinowski, M. Kamionkowski, and B. S. Sathyaprakash, Subtracting compact binary foregrounds to search for subdominant gravitational-wave backgrounds in next-generation ground-based observatories, *Phys. Rev. D* **108**, 064040 (2023).
- [35] M. Spera, M. Mapelli, N. Giacobbo, A. A. Trani, A. Bressan, and G. Costa, Merging black hole binaries with the SEVN code, *Mon. Not. R. Astron. Soc.* **485**, 889 (2019).
- [36] M. Mapelli, M. Spera, E. Montanari, M. Limongi, A. Chieffi, N. Giacobbo, A. Bressan, and Y. Bouffanais, Impact of the rotation and compactness of progenitors on the mass of black holes, *Astrophys. J.* **888**, 76 (2020).
- [37] G. Iorio, M. Mapelli, G. Costa, M. Spera, G. J. Escobar, C. Sgalletta, A. A. Trani, E. Korb, F. Santoliquido, M. Dall'Amico, N. Gaspari, and A. Bressan, Compact object mergers: Exploring uncertainties from stellar and binary evolution with SEVN, *Mon. Not. R. Astron. Soc.* **524**, 426 (2023).
- [38] P. Madau and T. Fragos, Radiation backgrounds at cosmic dawn: X-rays from compact binaries, *Astrophys. J.* **840**, 39 (2017).
- [39] T. Hartwig, M. Magg, L.-H. Chen, Y. Tarumi, V. Bromm, S. C. O. Glover, A. P. Ji, R. S. Klessen, M. A. Latif, M. Volonteri, and N. Yoshida, Public release of a-sloth: Ancient stars and local observables by tracing halos, *Astrophys. J.* **936**, 45 (2022).
- [40] J. Jaacks, S. L. Finkelstein, and V. Bromm, Legacy of star formation in the pre-reionization universe, *Mon. Not. R. Astron. Soc.* **488**, 2202 (2019).
- [41] B. Liu and V. Bromm, When did population III star formation end?, *Mon. Not. R. Astron. Soc.* **497**, 2839 (2020).
- [42] D. Skinner and J. H. Wise, Cradles of the first stars: Self-shielding, halo masses, and multiplicity, *Mon. Not. R. Astron. Soc.* **492**, 4386 (2020).
- [43] F. Santoliquido, M. Mapelli, Y. Bouffanais, N. Giacobbo, U. N. Di Carlo, S. Rastello, M. C. Artale, and A. Ballone, The cosmic merger rate density evolution of compact binaries formed in young star clusters and in isolated binaries, *Astrophys. J.* **898**, 152 (2020).
- [44] F. Santoliquido, M. Mapelli, N. Giacobbo, Y. Bouffanais, and M. C. Artale, The cosmic merger rate density of compact objects: Impact of star formation, metallicity, initial mass function, and binary evolution, *Mon. Not. R. Astron. Soc.* **502**, 4877 (2021).
- [45] <https://zenodo.org/records/7794546>.
- [46] <https://zenodo.org/records/8154846>.
- [47] I. Gupta, S. Borhanian, A. Dhani, D. Chattopadhyay, R. Kashyap, V. A. Villar, and B. S. Sathyaprakash, Neutron star-black hole mergers in next generation gravitational-wave observatories, *Phys. Rev. D* **107**, 124007 (2023).

- [48] C. García-Quirós, M. Colleoni, S. Husa, H. Estellés, G. Pratten, A. Ramos-Buades, M. Mateu-Lucena, and R. Jaume, Multimode frequency-domain model for the gravitational wave signal from nonprecessing black-hole binaries, *Phys. Rev. D* **102**, 064002 (2020).
- [49] V. Srivastava, D. Davis, K. Kuns, P. Landry, S. Ballmer, M. Evans, E. D. Hall, J. Read, and B. S. Sathyaprakash, Science-driven tunable design of cosmic explorer detectors, *Astrophys. J.* **931**, 22 (2022).
- [50] B. Sathyaprakash *et al.*, Scientific objectives of Einstein telescope, *Classical Quantum Gravity* **29**, 124013 (2012).
- [51] E. Pizzati, S. Sachdev, A. Gupta, and B. S. Sathyaprakash, Toward inference of overlapping gravitational-wave signals, *Phys. Rev. D* **105**, 104016 (2022).
- [52] S. Borhanian, GWBENCH: A novel Fisher information package for gravitational-wave benchmarking, *Classical Quantum Gravity* **38**, 175014 (2021).
- [53] H. Song, D. Liang, Z. Wang, and L. Shao, Impact of spin in compact binary foreground subtraction for estimating the residual stochastic gravitational-wave background in ground-based detectors, *Phys. Rev. D* **109**, 123014 (2024).
- [54] K. Belczynski, V. Kalogera, F. A. Rasio, R. E. Taam, A. Zezas, T. Bulik, T. J. Maccarone, and N. Ivanova, Compact object modeling with the STARTRACK population synthesis code, *Astrophys. J. Suppl. Ser.* **174**, 223 (2008).
- [55] C. Chiosi, A. Bressan, L. Portinari, and R. Tantalo, A new scenario of galaxy evolution under a universal initial mass function, *Astron. Astrophys.* **339**, 355 (1998).
- [56] T. Abel, G. L. Bryan, and M. L. Norman, The formation of the first star in the universe, *Science* **295**, 93 (2002).
- [57] V. Bromm and R. B. Larson, The first stars, *Annu. Rev. Astron. Astrophys.* **42**, 79 (2004).
- [58] N. Yoshida, K. Omukai, L. Hernquist, and T. Abel, Formation of primordial stars in a  $\Lambda$ CDM universe, *Astrophys. J.* **652**, 6 (2006).
- [59] V. Bromm, Formation of the first stars, *Rep. Prog. Phys.* **76**, 112901 (2013).
- [60] S. Glover, The first stars, in *The First Galaxies: Theoretical Predictions and Observational Clues*, edited by T. Wiklund, B. Mobasher, and V. Bromm (Springer, Berlin, 2013), pp. 103–174.
- [61] S. Goswami, L. Silva, A. Bressan, V. Grisoni, G. Costa, P. Marigo, G. L. Granato, A. Lapi, and M. Spera, Impact of very massive stars on the chemical evolution of extremely metal-poor galaxies, *Astron. Astrophys.* **663**, A1 (2022).
- [62] R. Schneider, K. Omukai, A. K. Inoue, and A. Ferrara, Fragmentation of star-forming clouds enriched with the first dust, *Mon. Not. R. Astron. Soc.* **369**, 1437 (2006).
- [63] A. Stacy and V. Bromm, Constraining the statistics of Population III binaries, *Mon. Not. R. Astron. Soc.* **433**, 1094 (2013).
- [64] H. Susa, K. Hasegawa, and N. Tominaga, The mass spectrum of the first stars, *Astrophys. J.* **792**, 32 (2014).
- [65] S. Hirano, T. Hosokawa, N. Yoshida, H. Umeda, K. Omukai, G. Chiaki, and H. W. Yorke, One hundred first stars: Protostellar evolution and the final masses, *Astrophys. J.* **781**, 60 (2014).
- [66] S. Hirano, T. Hosokawa, N. Yoshida, K. Omukai, and H. W. Yorke, Primordial star formation under the influence of far ultraviolet radiation: 1540 cosmological haloes and the stellar mass distribution, *Mon. Not. R. Astron. Soc.* **448**, 568 (2015).
- [67] K. M. J. Wollenberg, S. C. O. Glover, P. C. Clark, and R. S. Klessen, Formation sites of population III star formation: The effects of different levels of rotation and turbulence on the fragmentation behaviour of primordial gas, *Mon. Not. R. Astron. Soc.* **494**, 1871 (2020).
- [68] S. Chon, K. Omukai, and R. Schneider, Transition of the initial mass function in the metal-poor environments, *Mon. Not. R. Astron. Soc.* **508**, 4175 (2021).
- [69] A. Tanikawa, H. Susa, T. Yoshida, A. A. Trani, and T. Kinugawa, Merger rate density of population III binary black holes below, above, and in the pair-instability mass gap, *Astrophys. J.* **910**, 30 (2021).
- [70] O. Jaura, S. C. O. Glover, K. M. J. Wollenberg, R. S. Klessen, S. Geen, and L. Haemmerlé, Trapping of H II regions in population III star formation, *Mon. Not. R. Astron. Soc.* **512**, 116 (2022).
- [71] L. R. Prole, P. C. Clark, R. S. Klessen, and S. C. O. Glover, Fragmentation-induced starvation in population III star formation: A resolution study, *Mon. Not. R. Astron. Soc.* **510**, 4019 (2022).
- [72] J. Park, M. Ricotti, and K. Sugimura, Population III star formation in an X-ray background: III. Periodic radiative feedback and luminosity induced by elliptical orbits, *Mon. Not. R. Astron. Soc.* **521**, 5334 (2023).
- [73] P. Kroupa, On the variation of the initial mass function, *Mon. Not. R. Astron. Soc.* **322**, 231 (2001).
- [74] R. B. Larson, Early star formation and the evolution of the stellar initial mass function in galaxies, *Mon. Not. R. Astron. Soc.* **301**, 569 (1998).
- [75] B. Liu and V. Bromm, Gravitational waves from population III binary black holes formed by dynamical capture, *Mon. Not. R. Astron. Soc.* **495**, 2475 (2020).
- [76] H. Sana, S. E. de Mink, A. de Koter, N. Langer, C. J. Evans, M. Gieles, E. Gosset, R. G. Izzard, J. B. Le Bouquin, and F. R. N. Schneider, Binary interaction dominates the evolution of massive stars, *Science* **337**, 444 (2012).
- [77] Planck Collaboration, Planck 2015 results. XIII. Cosmological parameters, *Astron. Astrophys.* **594**, A13 (2016).
- [78] T. Hartwig, M. Magg, L.-H. Chen, Y. Tarumi, V. Bromm, S. C. O. Glover, A. P. Ji, R. S. Klessen, M. A. Latif, M. Volonteri, and N. Yoshida, Public release of A-SLOTH: Ancient stars and local observables by tracing halos, *Astrophys. J.* **936**, 45 (2022).
- [79] B. Uysal and T. Hartwig, First estimate of the local value of the baryonic streaming velocity, *Mon. Not. R. Astron. Soc.* **520**, 3229 (2023).
- [80] P. F. Hopkins, A new class of accurate, mesh-free hydrodynamic simulation methods, *Mon. Not. R. Astron. Soc.* **450**, 53 (2015).
- [81] P. Madau and M. Dickinson, Cosmic star-formation history, *Annu. Rev. Astron. Astrophys.* **52**, 415 (2014).
- [82] G. L. Bryan *et al.* (Enzo Collaboration), ENZO: An adaptive mesh refinement code for astrophysics, *Astrophys. J. Suppl. Ser.* **211**, 19 (2014).
- [83] S. E. Woosley, A. Heger, and T. A. Weaver, The evolution and explosion of massive stars, *Rev. Mod. Phys.* **74**, 1015 (2002).
- [84] G. Volpato, P. Marigo, G. Costa, A. Bressan, M. Trabucchi, and L. Girardi, A study of primordial very massive star evolution, *Astrophys. J.* **944**, 40 (2023).